REVISTA MATÉRIA V.27 N.03
ISSN 1517-7076 articles e20220002, 2022

Influence of test parameters on the cyclic oxidation behavior of AISI 310 and a new Fe-5.9Si-3.9Cr-4.5Ni-0.8C (wt.%) alloy

João Gabriel da Cruz Passos[1,2], Daniele Silva[2], Robson Bruno Dutra Pereira[2], Artur Mariano de Sousa Malafaia[2]

[1]Universidade de São Paulo, Escola de Engenharia de São Carlos, Departamento de Engenharia de Materiais, Laboratório de Solidificação. Av. João Dagnone, 1100, Jardim Santa Angelina, 13563-120, São Carlos, SP, Brasil.

[2]Universidade Federal de São João del-Rei, Departamento de Engenharia Mecânica e de Produção, Laboratório de Oxidação. Praça Frei Orlando, 170, Centro, 36307-334, São João del-Rei, MG, Brasil.

e-mail: jgpassos@usp.br, danny-silvaa@hotmail.com, robsondutra@ufsj.edu.br, arturmalafaia@ufsj.edu.br

ABSTRACT

High-temperature cyclic oxidation is governed by various cycle parameters (maximum temperature, cooling and heating rates, exposure time at high temperature) and atmosphere (composition, temperature, and pressure), complicating the evaluation of the effect of each parameter by itself. This study used a factorial design to evaluate three influential parameters in cyclic oxidation: alloy composition, upper dwell time (UDT), and surface finish. The method requires fewer experiments than ones previously used and can identify interactions between parameter effects. Two alloys, a ferritic Fe-5.9Si-3.9Cr-4.5Ni-0.8C (FeSiCr) alloy and conventional austenitic stainless steel AISI 310 were exposed to air at 950 °C for 100 h. Two different surface finishes (#220 and #600 SiC sandpaper) and two UDTs (30 and 60 minutes) were used. Mass variation data from eight different exposure times and metal/oxide interface roughness were analyzed. The FeSiCr alloy oxide layer was also characterized to complement the statistical analysis results. It was observed that different test stages were governed by different parameters. The surface finish was relevant at the beginning of the test, whereas UDT was relevant at the end. Interactions were irrelevant thorough the test. FeSiCr presented a promising behavior, with similar mass variation and higher oxide spallation resistance than AISI 310.

Keywords: Cyclic oxidation; FeSiCr alloy; Factorial design; Surface finish.

1. INTRODUCTION

Alloy composition is an influential parameter in oxidation, serving as a predictor for how a given alloy will behave under these conditions. First, it determines the substrate phase in iron-based alloys (austenite/ferrite). This is relevant because, during cooling, the metal tends to contract more than the oxide layer, generating stresses that can initiate defects and cause oxide spallation. The difference in contraction is related to a coefficient of thermal expansion (CTE) mismatch between metal and oxide. Therefore, austenitic alloys (higher CTE) are more prone to spallation than ferritic ones [1–2]. Furthermore, oxidation rates are reliant on oxide layer composition, also related to alloy composition. For this reason, aluminum and/or chromium addition is used to increase high-temperature oxidation resistance in most Ni-based superalloys [3] and Fe-based stainless steels often use chromium [4]. Additionally, silicon-alloyed Fe-based alloys can exhibit protective SiO_2 oxide formation [5], and silicon synergizes well with chromium when a certain amount of both is present in an alloy [4–7]. Silicon has been recently used, for example, to increase the oxidation resistance of chromium-containing high-entropy alloys [8–10]. Iron-based alloys with around 15 wt.% silicon showed high corrosion and oxidation resistance [11–13], but poor machinability and conformability limited their application [11–12]. Silicon content is thus often limited in iron-based alloys (up to 2 wt.% in general) to improve the oxidation resistance of chromia-forming stainless steels (over 11 wt.% chromium) [14]. Considering the positive effects of both elements on the oxidation resistance of ferrous alloys, an alloy with moderate amounts of Si and Cr (5.5 and 5 wt.%, respectively) was presented and tested in a previous study of our group. After oxidation for up to 76 cycles at 950 °C in air, the alloy formed $MnCr_2O_4$ and Cr_2O_3 oxides, a promising result that indicated the possibility of creating oxidation-resistant Fe-Si-Cr alloys with such an approach [4]. Based on these results, another study evaluated the effect of silicon and chromium on the oxidation behavior of three FeSiCr alloys, confirming that moderate

Corresponding Author: Joao Gabriel da Cruz Passos Received on 08/02/2022 Accepted on 19/04/2022

DOI: https://doi.org/10.1590/1517-7076-RMAT-2022-0002

amounts of silicon and chromium (less than 6 wt.% of each) are indeed capable of being used in the creation of oxidation-resistant alloys [15].

The aforementioned studies relate the cyclic oxidation behavior of FeSiCr alloys to temperature and time (in the form of several cycles of fixed duration). Cyclic oxidation, however, is governed by several other parameters; therefore, for a comprehensive characterization of the oxidation behavior of the FeSiCr alloy, further studies are required. The determination and prediction of the effects that determine cyclic oxidation behavior, which was attempted in previous studies, is also essential for the generalization of experimental results, facilitating comparisons between different alloys [16–18]. One of those investigations used statistical analysis, applying an experimental design that defined the main effect of each parameter, but not how they interacted with each other. Also, this study evaluated the oxidation behavior after the end of the test, not on a cycle-by-cycle basis [19]. The discussed research is part of a series of studies that analyzed cyclic oxidation experiments to identify and quantify the effects of experimental parameters [20]. These studies culminated in the creation of a standard for cyclic corrosion tests, ISO 13573:2012. Although this standard helps in obtaining concise results among different research groups, it does not discuss behavior prediction via statistical analyses.

One of the other parameters besides alloy composition that affects cyclic oxidation is surface roughness. As a previous study has shown, evaluating oxidation resistance without control over the initial surface condition can yield misleading results [21]. A rougher surface has a larger area directly exposed to oxygen, and the volume-to-surface ratio affects cooling rates [22]. A rough pre-oxidation surface also reduced the adherence of alumina scales on MA 956 alloy [23]. A study on steam oxidation of stainless steels at 650 and 700 °C, however, showed higher oxidation resistance of samples with a 600-grit finish than of polished ones [24]. Samples of TiAl alloys with a 600-grit finish also had slower oxidation rates than polished ones at 900 °C when exposed to pure oxygen. On the other hand, when they were exposed to air, no significant difference between oxidation rates was observed [25]. Finally, the oxidation process itself can increase metal/oxide interface roughness. During cyclic oxidation of some FeMnSiCrNi alloys, this increase in roughness induced new mass gain after an initial spallation period [26–28]. However, in an oxide-strengthened Fe_3Al alloy, the metal/oxide interface roughness increase during cyclic oxidation led to an increase in mass loss [29].

Another controllable parameter in cyclic oxidation, high-temperature dwell time per cycle or upper dwell time (UDT), had no statistical influence on the mass variation of FeCrAl alloys at 600 h of exposure (UDTs of 2, 20, or 100 h at 1200 °C). However, when combining results from various data sources, it was observed that longer UDTs increased mass gain for 100 and 500 h of exposure [30]. A shorter UDT reduced the time for spallation onset in Fe-based 800H alloy at 950, 1000 and 1050 °C (UDTs between 0.5 and 5 h) and in Fe-based AISI 441 alloy at 800, 850 and 900 °C (UDTs between 4 and 20h) [31]. The opposite behavior (longer UDTs facilitating spallation) was observed in NiCr alloys at 1000 °C, for an equal number of cycles. The effect was dependent on alloy composition [32]. The UDT effect was also evaluated with a statistical model applied to Ni-based superalloys oxidized at 1000 °C, which indicated that longer UDTs increase spallation probability [33].

Considering the promising results of alloys with moderate silicon and chromium contents, this paper evaluated the cyclic oxidation behavior of non-commercial ferritic Fe-5.9Si-3.9Cr-4.5Ni-0.8C (FeSiCr) alloy and related it to surface finish and UDT. This alloy was compared with a more expensive conventional austenitic stainless steel AISI 310. A factorial design was used, which required only one replicate and could statistically determine parameter effects and interactions. Mass variation and final metal/oxide surface roughness were used as response parameters and the oxide layers were characterized.

2. MATERIALS AND METHODS

The origin and preparation of the alloys were discussed in previous studies from our group [4, 15], in which a promising behavior of FeSiCr compared to 310 was observed, motivating this investigation. The chemical composition of FeSiCr alloy in wt.%, determined by arc spark Optical Emission Spectrometer is Fe–5.9(±0.040) Si–3.85(±0.021) Cr–4.5(±0.038) Ni–0.79(±0.0044) Mn–0.76(±0.0073) C [15]. FeSiCr presented a better behavior than another alloy containing less Si and similar content of the other elements [15]. The samples used in this study had a surface area of approximately 5 cm². To standardize surface finishing, the rectangular samples were sanded up to 220 or 600-grit SiC sandpaper. The UDT was controlled by a programmed furnace maintained at 950 °C during the test, based on the cycling parameters shown in Figure 1. The UDT consisted of 30 or 60 minutes of heating and maintenance at the dwell temperature (T_d, 950 °C). Thus, the heating time (t_h) was considered part of the UDT. The cooling interval consisted of a 5-minute period in which the furnace moved, exposing the samples to ambient temperature. The samples are then cooled to a low temperature (T_l). The samples were oxidized in laboratory air atmosphere.

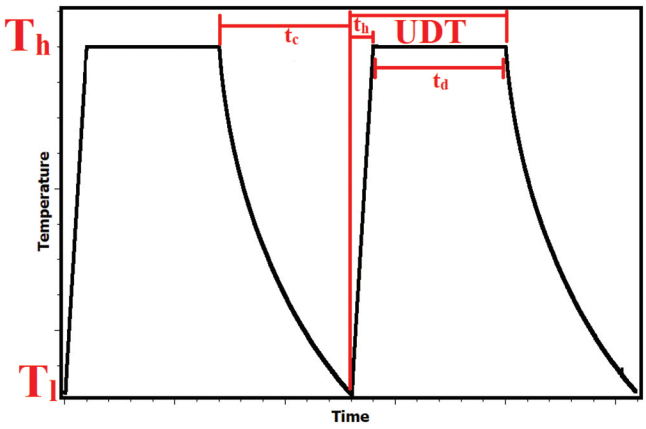

Figure 1: Schematic of the cyclic oxidation tests performed in this study. The oxidation occurs at a high temperature (T_h) and the sample is cooled to a low temperature during each cycle (T_l). The cycle consists of the time the sample is kept at the high temperature (t_h) and the cooling and heating times (t_c and t_h), the cooling time is fixed at 5 minutes, and the heating time of the time taken for the sample to reach the upper temperature. Because t_h is very short, it was considered as part of the UDT together with t_d. Note that the time scale does not reflect the real test, it was presented in this manner to facilitate visualization.

Each sample was weighed before oxidation and after a cumulative UDT of 5 and 10 h. In sequence, measurements were made in 15-hour intervals up to a cumulative UDT of 100 h, totaling 8 observation points. Spalled oxides were not weighed; therefore, the results concern the net (not gross) mass variation. Samples with a 60-minute UDT were exposed to 100 cycles, and samples with a 30-minute UDT, 200 cycles. A previous study, using another experimental design, evaluated that a minimum exposure time of 300 h is required for reliable results (it also required multiple replicates per experimental parameter) [19]. The present study, however, evaluated the influence of test parameters in relation to exposure time. Thus, by discussing times below the 300-hour threshold, the possibility of studying early oxidation behavior with the use of a different experimental design is evaluated. After being oxidized, the samples were cross-sectioned and analyzed via Scanning Electron Microscopy (SEM) and Energy Dispersive X-Ray Spectroscopy (EDS). The oxidized surface of the alloys was also analyzed via SEM-EDS. The metal/oxide interface roughness (Ra and Rz) after 100 hours was measured with the ImageJ® software, using SEM images. An interface length of 1600 μm was used for each measurement. Surface roughness before oxidation was measured with a profilometer.

Statistical analysis was based on a 2k factorial design with k = 3 factors ($2^3 = 8$ experiments, as shown in Table 1). Linear regression models were calculated for each observation point. The model evaluated every main effect and excluded third-order interactions to allow estimation of the experimental error without replicates. Second-order interactions were considered only if they showed statistical relevance or their inclusion benefited the model fit. Table 2 shows the low and high levels of each parameter. The responses evaluated were mass variation per surface area and metal/oxide surface roughness.

3. RESULTS AND DISCUSSION

3.1. Mass variation and samples characterization

The mass variation as a function of test duration in each test condition is shown in Figure 2. Dwell time corresponds to the total time a given sample spent at the oxidation temperature (950 °C). The results indicate that FeSiCr gained more mass, but there were no clear signs of spallation, whereas AISI 310 samples started showing signs of spallation after 40 h, i.e. the mass variation turns negative, with a net weight reduction on subsequent mass measurements. Although AISI 310 has a higher spallation resistance than other austenitic stainless steels, it has already shown a tendency to spall in previous studies in which it was exposed to cyclic oxidation conditions at 950 °C and cooled in open air [34]. Further discussions regarding parameter effects on the mass variation will be presented in the following sections on a statistical basis.

The tendency for spallation in the AISI 310 alloy can also be verified by analyzing the oxidized surfaces of the samples. Figure 3 shows SEM images of the samples of FeSiCr and AISI 310 oxidized in 30-minute cycles with an initial surface finish of 220-grit. The FeSiCr sample does not show signs of spallation, while on the AISI 310 sample, some regions of spalled oxide can be observed. These regions can be easily observed via

Table 1: Experimental design consisting of three parameters varying between low (–1) and a high (1) level (8 different combinations).

EXPERIMENT	ALLOY	UDT	SURFACE FINISH
1	−1	−1	−1
2	−1	−1	1
3	−1	1	−1
4	−1	1	1
5	1	−1	−1
6	1	−1	1
7	1	1	−1
8	1	1	1

Table 2: Low (−1) and high (1) levels of each parameter (alloy, UDT and surface finish). Units of measurement are also presented. For surface finish, the low level consists of the rougher surface and for UDT, it consists of the shorter cycles. For the alloy parameter, levels were assigned arbitrarily.

PARAMETER	−1	1	UNIT
Alloy	FeSiCr	310	None
UDT	30	60	Minutes
Surface Finish	220	600	Sandpaper Grit

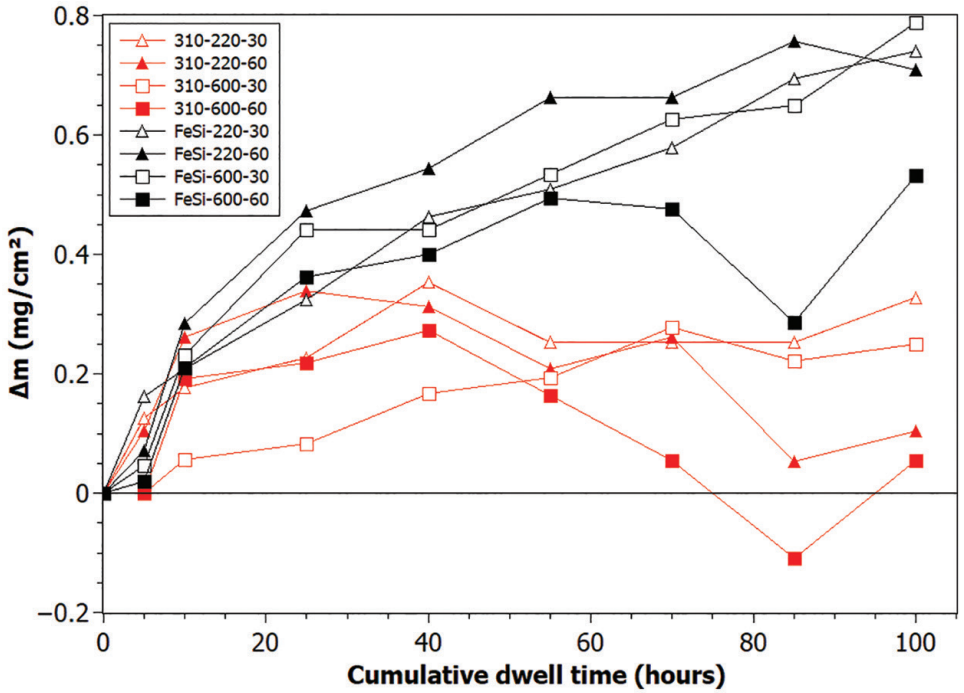

Figure 2: Mass variation curves for all test conditions. Each label follows the following format: Alloy – Surface Finish – UDT (continuous lines are simply visual guides and do not represent intermediate mass variation values between two measurement points).

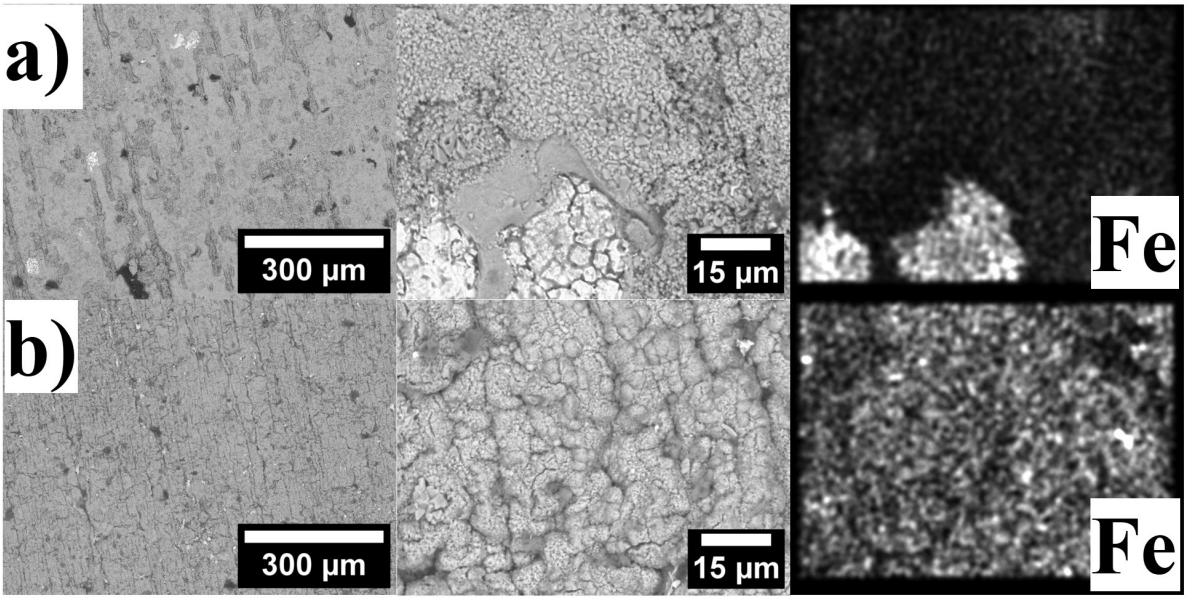

Figure 3: SEM images of the oxidized surface of samples of AISI 310 (a) and FeSiCr (b) exposed to 30-minute cycles with an initial surface finish of 220-grit. Low magnification on the left side, high magnification on the center and Fe EDS maps on the right side. The Fe maps show that there are regions in which the oxide spalled on the AISI 310 sample (a high iron content is characteristic of the metallic substrate exposed by spallation). On the FeSiCr sample, on the other hand, iron distribution is uniform and occurs only due to the interaction depth characteristic of EDS analyses (and is thus related to the substrate).

the EDS map of iron, as they have a high iron content, which is characteristic of the substrate (iron oxides were not observed in any of the alloys, as will be discussed in sequence). On the FeSiCr alloy, on the other hand, iron distribution is uniform, and the presence of the element occurs only due to the penetration depth of the EDS analysis. The same characteristics were observed in the samples tested in the other conditions (with different UDTs and initial surface finishes), with AISI 310 always presenting spallation, while FeSiCr did not.

EDS mapping on the cross-section of the conventional AISI 310 steel samples after 100 h of exposure showed appreciable amounts of Si, Cr and Mn in the oxide layer. The literature reports Cr_2O_3 and Cr-Mn spinel ($MnCr_2O_4$) formation during high-temperature oxidation of AISI 310 [35–37], with SiO_2 formation in some cases at the metal/oxide interface [37]. The EDS maps are not presented here because the AISI 310 alloy was thoroughly studied in various oxidation conditions in previous works [34–37], and the objective of its inclusion in this study is not to characterize its oxide layer but to compare its behavior to the FeSiCr alloy. Figure 4 shows SEM images and EDS mapping for the FeSiCr alloy. A discontinuous oxide layer was present in some cases (notable in Figure 4c), but these defects were unable to cause considerable spallation (as suggested by the mass variation results), indicating a promising spallation resistance. Manganese and chromium were the main elements present in the oxide layer. Chromium seems to appear as an oxide (Cr_2O_3) and part of a Mn-Cr spinel, since chromium was found in regions with high manganese content. A predominant Mn-Cr spinel ($MnCr_2O_4$) was observed in previous studies which evaluated this alloy in cyclic oxidation at 950 °C [4, 15]. There are also regions with high silicon and oxygen content, possibly evidence of silica formation. However, detecting this oxide is difficult, as it can be amorphous and of nanometric thickness [38–39]. In a previous study with this alloy, small regions with high silicon content were also observed and associated with probable silica formation [15]. According to a previous investigation on the FeSiCr alloy, silicon aids the formation of a protective Cr_2O_3 layer even with a low (below 4 wt.%) chromium content. As previously mentioned, silicon has the potential for increasing oxidation resistance by acting as a diffusion barrier, slowing the growth of chromium and iron oxides in FeSiCr alloys and facilitating the formation of a continuous protective Cr_2O_3 layer. Furthermore, the $MnCr_2O_4$ spinel that forms on the surface of the Cr_2O_3 layer can prevent chromium evaporation by stopping the transition of Cr_2O_3 to CrO_3, increasing oxidation resistance [15]. In the present study, it was shown that this oxidation mechanism is observed in this alloy at 950 °C for at least 85 cycles, independently of UDT and surface finish before oxidation.

The formation of a silicon-rich oxide is clearer in Figure 5, presenting the cross-section of the FeSiCr sample exposed to 30-minute cycles with a 220-grit surface finish at a higher magnification than in Figure 4. The EDS maps for iron, silicon and oxygen are shown. There is a region between the outer oxide layer and the

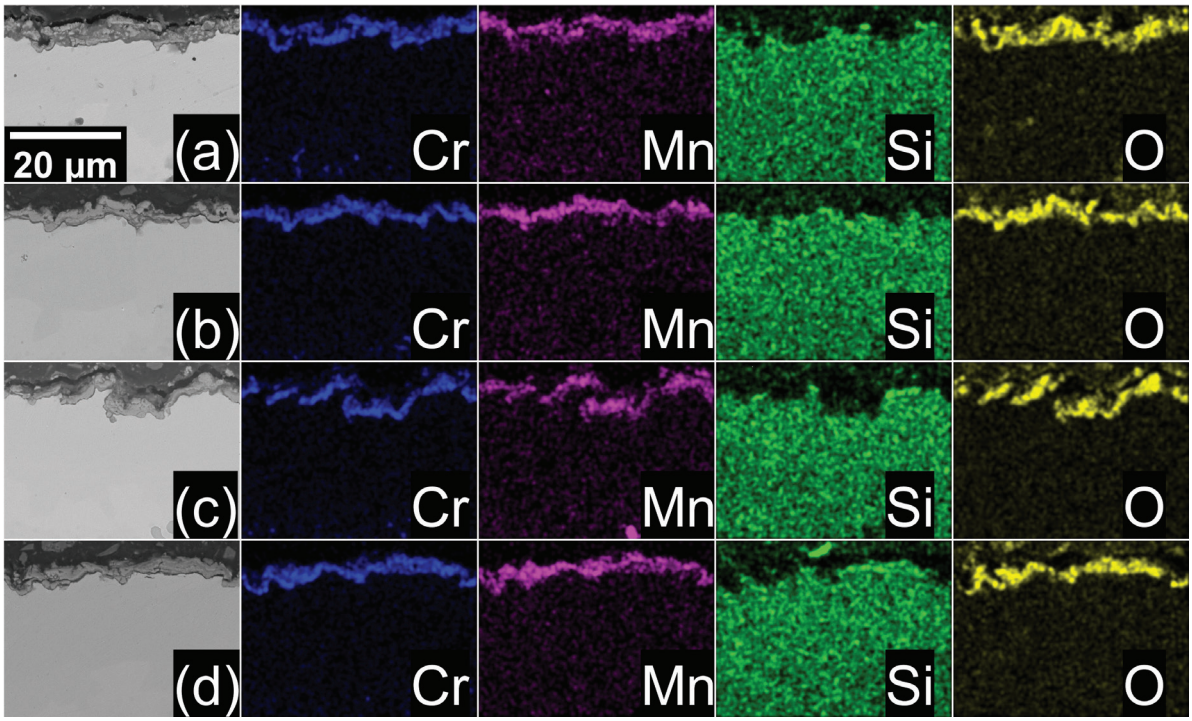

Figure 4: Cr, Mn, Si and O EDS maps of the oxide layer formed in FeSiCr alloy at each test condition after 100 h of total dwell time at 950 °C. Figures corresponds to the tests as follows: (a) 220 grit-60 minutes; (b) 220 grit-30 minutes; (c) 600 grit-60 minutes; and (d) 220 grit-60 minutes.

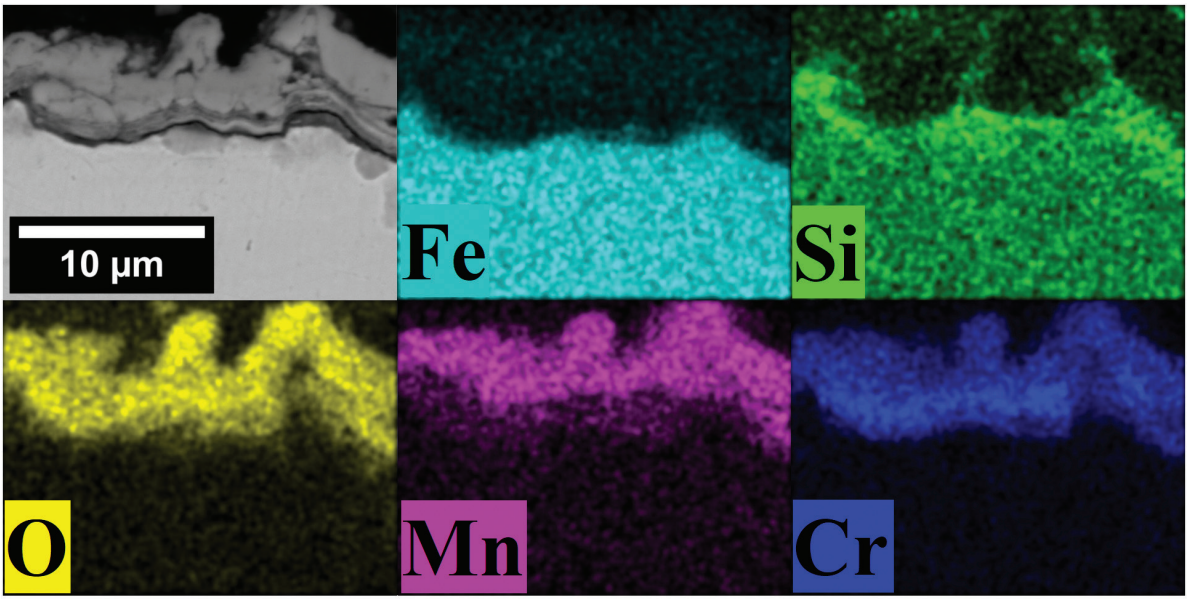

Figure 5: Fe, Si and O EDS maps of the oxide layer formed in FeSiCr alloy exposed to 30-minute cycles with an initial surface finish of 220-grit. The Si map shows a silicon-enriched region in which oxygen content is high and iron content is low, indicating the probable formation of silicon oxide.

metallic substrate in which the oxygen content is significant, indicating the presence of an oxide. The lack of iron is another indication that this region indeed consists of an oxide. This oxide layer is also silicon-enriched, which agrees with the results from previous studies and indicates that there is SiO_2 formation.

Considering that the metal/oxide interface roughness was an influential parameter in previous studies [26, 29], the interface roughness after 100 h oxidation was measured, as well as the initial surface roughness (Table 3). The measurements showed that the metallic surface increased during the oxidation process, and this

Table 3: Average initial and final Ra and Rz roughness values for samples of FeSiCr and 310 alloys with 220 and 600 grit surface finish. Although there are 8 different experimental conditions, initial roughness was measured only in four samples, as it was assumed that the initial roughness was the same in samples of the same alloy and with the same surface finishing. After oxidation, surface roughness was measured for each experimental condition, as UDT could now be a relevant parameter.

ALLOY	SURFACE FINISH	UDT	METALLIC SURFACE ROUGHNESS Ra [μm]		METALLIC SURFACE ROUGHNESS Rz [μm]	
			BEFORE OXIDATION	AFTER OXIDATION	BEFORE OXIDATION	AFTER OXIDATION
FeSiCr	220	30	0.22	3.71	1.50	15.53
		60	0.22	4.69	1.50	18.56
	600	30	0.04	3.44	0.28	13.19
		60	0.04	3.25	0.28	14.92
310	220	30	0.18	1.17	1.28	8.78
		60	0.18	1.17	128	6.58
	600	30	0.05	0.76	0.36	4.90
		60	0.05	1.05	0.36	6.46

increase was more significant in FeSiCr samples than that in 310 samples. Those results will be further discussed based on the statistical analysis.

3.2. Statistical analysis

Table 4 shows the estimated coefficients (column "Estimate") for the main effects and second-order interactions at 100 h. The "(Intercept)" value is a constant value associated with the average response but not related to any specific parameter. The linear coefficients are designed by β_i (with i = 0, 1, 2, or 3, corresponding to the intercept, UDT, surface finish, and alloy, respectively), as shown in Table 4. Interactions are defined by β_{ij}, corresponding to an interaction between parameters i and j. Each β has an associated p-value, related to the standard error and t-value. For this study, it was considered that a p-value lower than 0.05 indicates that the associated effect or interaction has strongly influenced the response (95% confidence interval); values between 0.05 and 0.1 indicate a statistically relevant but weaker influence (90% confidence interval). Second-order interactions, for example, were not statistically relevant, as their p-values were significantly higher than 0.1. The analysis discussed in this paragraph was applied to mass variation in each observation point and metal/oxide interface roughness after 100 hours of oxidation. In each case, a better combination of factors and interactions was included in the model based on fit and normality, such that some irrelevant second-order interactions were removed. Still, at some observation points, statistically insignificant interactions were kept, as the model had a better fit (higher R adjusted) with their inclusion. Statistically significant parameters are bolded in Tables 4 and 5.

Table 5 shows the statistical analysis results for each observation point. The values for 100 h are different from Table 4 because the interactions β_{13} and β_{23} were removed, increasing the Adj-R^2 from 0.9063 to 0.9605. The p-values for each estimated effect in all conditions used for statistical analysis are in Table 5, in column p-value (Estimate), as well as the fit of each regression model (Adj. R^2). The Adj. R^2 was very low at 10 and 25 h; therefore, they were deemed unfit for statistical analysis. Table 5 shows a significant alloy composition impact in mass variation from 40 to 100 h, and also for metal/oxide interface roughness at the end of the test. Dwell periods in which surface finish (5 and 40 h) and UDT (85 and 100 h) had a significant impact on mass variation were also observed. Finally, no lack of normality was observed in the residuals, as the p-values for the Shapiro-Wilk normality test are all higher than 0.05, indicating that the null hypothesis (normality) can be assumed.

3.3. Alloy influence

The main effect plots for the samples exposed to high temperature for 100 h are shown in relation to mass variation (delta mass) in Figure 6 and metal/oxide interface roughness (Ra) in Figure 7. As observed in Table 5,

Table 4: Statistical analysis of the main effects and interactions after 100 h of total dwell time. Statistically relevant values (p-value < 0.1) are bolded. Also shown are the estimated coefficients, the standard deviations and t-values.

β	ESTIMATE	STD. ERROR	T-VALUE	P-VALUE (ESTIMATE)
Main Effects				
(Intercept) (β_0)	0.438509	0.031779	13.799	**0.0461**
UDT (β_1)	−0.08826	0.031779	−2.777	0.22
Surface finish (β_2)	−0.0321	0.031779	−1.01	0.4968
Alloy (β_3)	0.254479	0.031779	8.008	**0.0791**
Interactions				
β_{12}	−0.02458	0.031779	−0.773	0.5809
β_{13}	0.016385	0.031779	0.516	0.6969
β_{23}	–0.00013	0.031779	–0.004	0.9974

Table 5: Main effects and interactions used for each statistical analysis. Statistically relevant values (p-value < 0.1) are bolded. Also shown are the estimated coefficients, the standard deviations and t-values. The Adj. R^2 values and p-values of the Shapiro-Wilk tests, used to determine which regressions were adequate, are shown for each test condition (a p-value higher than 0.05 indicates normality).

OBS. TIME (HOURS)	β	ESTIMATE	STD. ERROR	T-VALUE	P-VALUE (ESTIMATE)	ADJ. R^2	P-VALUE (SHAPIRO-WILK)
5	β_0	0.066085	0.009336	7.078	**0.0021**	0.8095	0.08848
	β_1	–0.01755	0.009336	−1.88	0.1333		
	β_2	–0.04973	0.009336	−5.326	**0.00598**		
	β_3	0.008524	0.009336	0.913	0.41278		
10	β_0	0.20213	0.01677	12.052	**0.000272**	0.5277	0.9511
	β_1	0.03403	0.01677	2.029	0.112302		
	β_2	–0.03015	0.01677	−1.798	0.146613		
	β_3	0.03124	0.01677	1.863	0.135949		
25	β_0	0.30832	0.0286	10.781	**0.00042**	0.5986	0.5757
	β_1	0.03954	0.0286	1.383	0.23893		
	β_2	–0.03234	0.0286	−1.131	0.32134		
	β_3	0.09154	0.0286	3.201	**0.03287**		
40	β_0	0.36904	0.01667	22.135	**3.5e-06**	0.8432	0.2684
	β_2	–0.0491	0.01667	−2.945	**0.0320**7		
	β_3	0.0928	0.01667	5.566	**0.00258**		

(*Continued*)

Table 5: Continue

OBS. TIME (HOURS)	β	ESTIMATE	STD. ERROR	T-VALUE	P-VALUE (ESTIMATE)	ADJ. R^2	P-VALUE (SHAPIRO-WILK)
55	β_0	0.377285	0.020859	18.087	**5.49E-05**	0.9064	0.8225
	β_1	0.004976	0.020859	0.239	0.82316		
	β_2	–0.03075	0.020859	−1.474	0.21449		
	β_3	0.172681	0.020859	8.279	**0.00116**		
70	β_0	0.39844	0.3062	13.01	**0.000201**	0.8425	0.1008
	β_1	–0.03523	0.3062	−1.15	0.314116		
	β_2	–0.03997	0.3062	−1.305	0.261855		
	β_3	0.18734	0.3062	6.117	**0.003616**		
85	β_0	0.35041	0.04664	7.512	**0.00168**	0.8269	0.6118
	β_1	–0.10413	0.04664	−2.232	**0.08937**		
	β_2	–0.08852	0.04664	−1.898	0.13058		
	β_3	0.24621	0.04664	5.279	**0.00618**		
100 (Δm)	β_0	0.43851	0.02064	21.243	**0.000228**	0.9605	0.2948
	β_1	–0.08826	0.02064	−4.276	**0.023493**		
	β_2	–0.0321	0.02064	−1.555	0.217817		
	β_3	0.25448	0.02064	12.328	**0.001150**		
	β_{12}	−0.02458	0.02064	−1.191	0.319462		
100 (Ra)	β_0	2.4044	0.1358	17.707	**0.00317**	0.9366	0.1225
	β_1	0.1326	0.1358	0.991	0.42595		
	β_2	−0.2786	0.1358	−2.052	0.17661		
	β_3	1.3676	0.1358	10.072	**0.00971**		
	β_{12}	−0.1099	0.1358	−0.809	0.50337		
	β_{23}	−0.1469	0.1358	−1.082	0.39247		
100 (Rz)	β_0	11.160	0.4305	25.818	**0.000127**	0.9753	0.9465
	β_1	0.5139	0.4305	1.194	0.318378		
	β_2	−1.2482	0.4305	−2.899	**0.062551**		
	β_3	4.4347	0.4305	10.300	**0.001952**		
	β_{13}	0.6755	0.4305	1.569	0.214684		

"alloy" was the most influential parameter in the final mass variation and metal/oxide surface roughness, with higher mass gain for FeSiCr alloy. Adding "Alloy" as a parameter was necessary, even if its influence on mass variation is expected due to chemical composition differences. A study with only two parameters would require replicates to be able to identify interactions between parameters. Also, identifying an interaction between a given parameter and alloy composition would show that this parameter had a different effect on the oxidation behavior of each alloy. Finally, the model can be used to quantify the difference in oxidation resistance between the alloys.

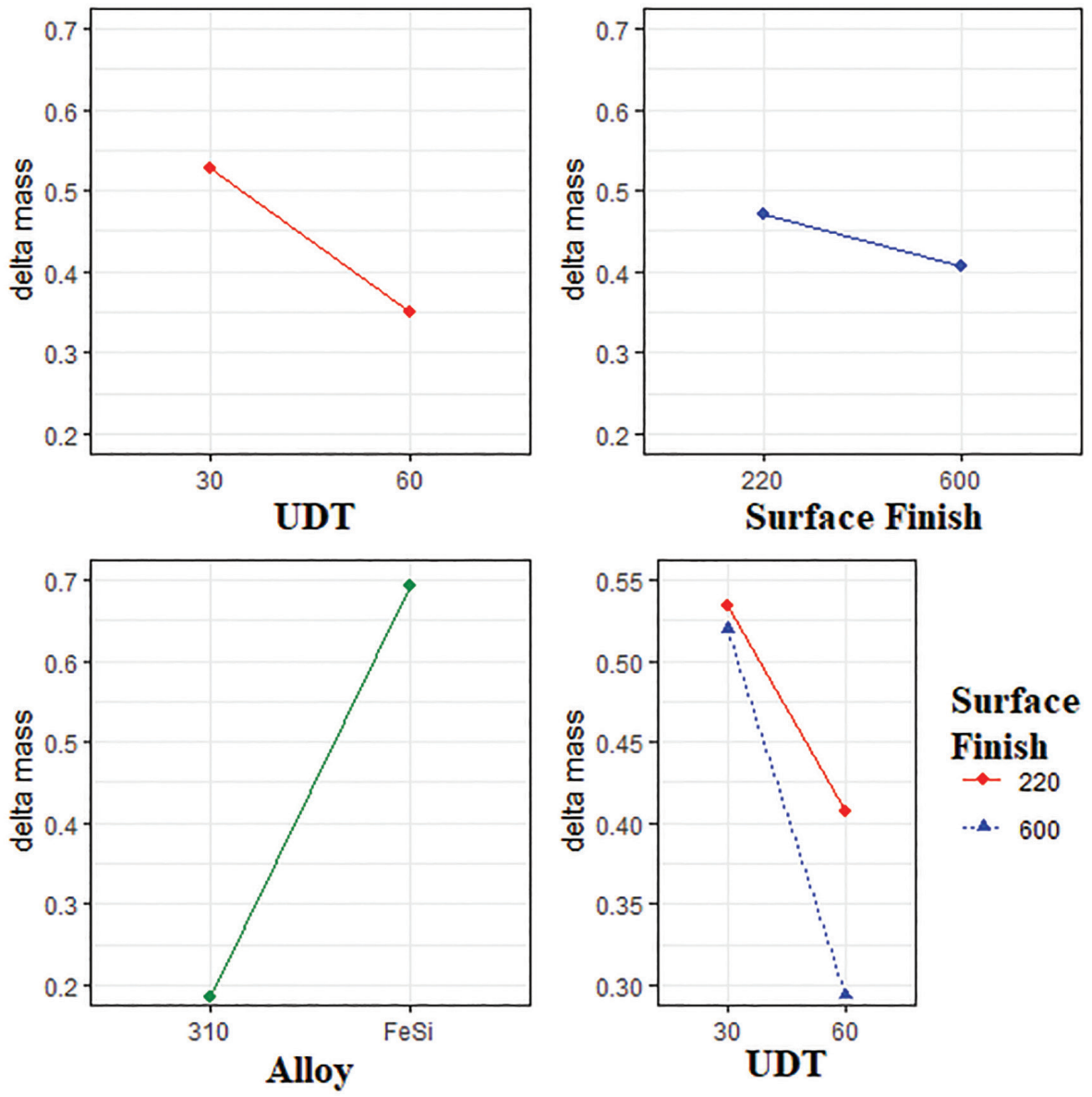

Figure 6: Main parameter effects and interaction plots for the mass variation response after 100 h of total dwell time. The extremities of each line indicate the average mass variation when the parameter is at a given level. Positive slopes indicate that changing the parameter from the lower to the upper level tends to increase mass variation, and negative slopes indicate that such a change tends to decrease mass variation, on average (note that the effect is not necessarily statistically relevant, as Table 5 shows).

Alloy composition was statistically relevant for every point of observation except 5 h. The lack of significance at 5 h shows that FeSiCr and 310 behaved similarly during the first hours. For the remainder of the test, the conventional 310 stainless steel gained less mass. This was caused by the higher chromium content in 310 and agrees with a previous study comparing both alloys [4]. After 40 h, signs of spallation were observed in 310 but not in FeSiCr. Mass spallation during cyclic oxidation was already observed in the 310 alloy [4]. Alloy FeSiCr resisted spallation in a previous study at 950 °C in which the samples were oxidized for a shorter total time (47 h) [15], but this alloy suffered significant mass spallation when exposed to 60-minute UDTs with 10-minute cooling intervals [4]. As shown in Figure 1, the lower temperature is determined by the cooling interval; therefore, longer cooling periods increase the temperature gradient, and consequently the thermal stresses generated at the oxide layer, which may explain the better oxide stability here, with 5-minute cooling intervals. However, the samples were cooled to room temperature when weighed at the observation points, generating the maximum temperature gradient possible for these conditions. Nonetheless, the results show that, compared to the austenitic 310 alloy, the ferritic FeSiCr alloy had a higher spallation resistance. This behavior is most likely related to the previously mentioned CTE differences between austenitic and ferritic substrates which leads to a higher tendency for spallation in austenitic alloys.

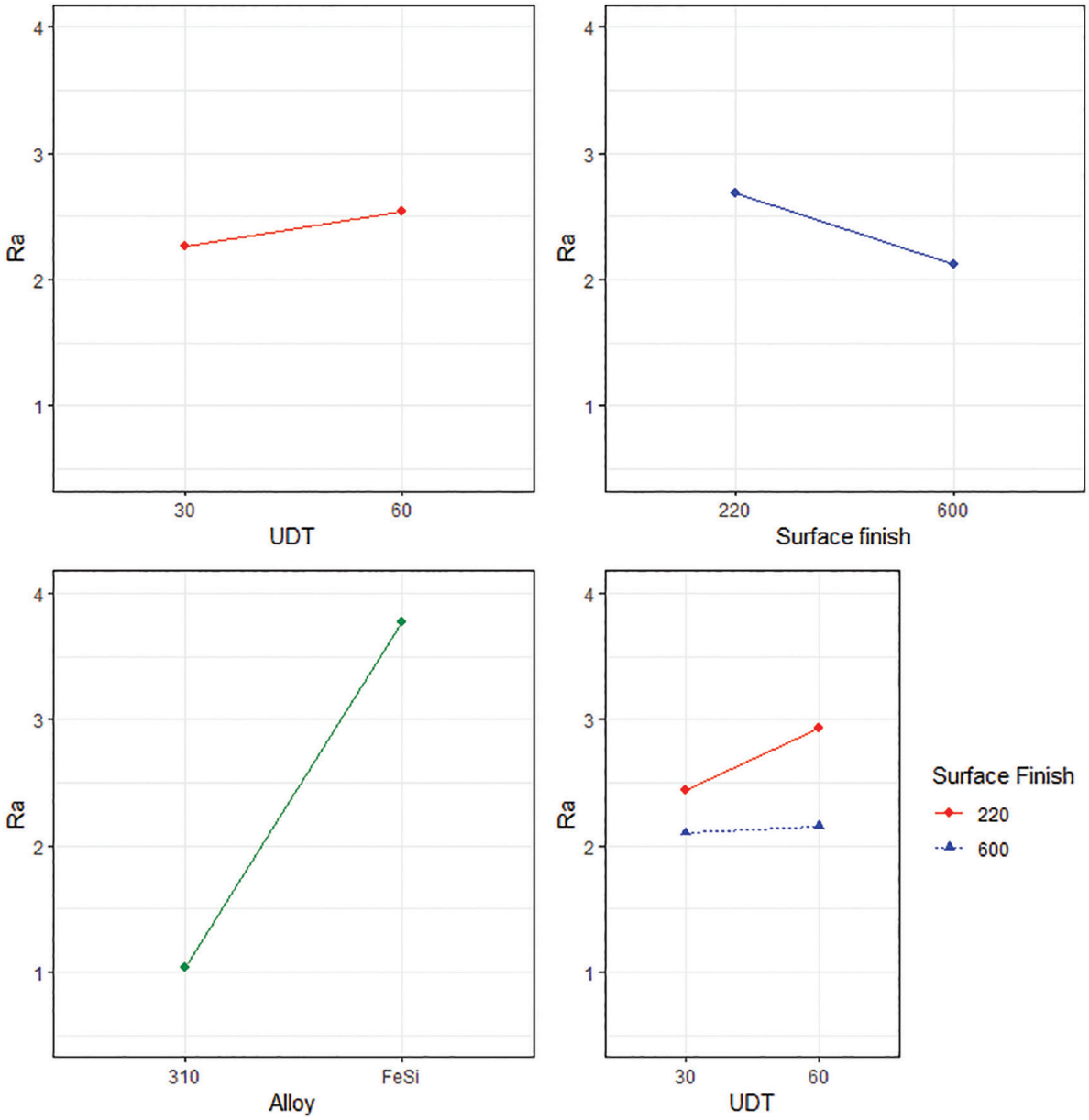

Figure 7: Main parameter effects and interaction plots for the metal/oxide interface roughness (Ra) response after 100 h of total dwell time. The extremities of each line indicate the average roughness when the parameter is at a given level. Positive slopes indicate that changing the parameter from the lower to the upper level tends to increase roughness, and negative slopes indicate that such a change tends to decrease roughness, on average (note that the effect is not necessarily statistically relevant, as Table 5 shows).

The "Alloy" parameter was also strongly significant for metal/oxide interface roughness (both Ra and Rz), showing that FeSiCr alloy forms rougher interfaces after oxidation. This roughness increase is related to a chemical effect that occurs when oxide-forming elements are depleted from the substrate, and oxygen can diffuse into the metallic substrate and form "peaks" of oxide that grow inwards. Considering that the FeSiCr alloy has a lower chromium content (the main oxide-forming element), chromium depletion was more significant than in the 310 alloy. Also, FeSiCr alloy probably formed more oxides (as it gained more mass), further increasing chromium depletion. Thus, the roughness increase due to the chemical effect was more significant. A previous study has shown that this effect influences oxidation behavior, increasing oxide layer-substrate adherence [26]. Therefore, this effect may have increased FeSiCr spallation resistance.

3.4. Surface finish influence

Statistical analysis showed no statistically relevant difference between the mass gain between samples with a 220 grit and a 600-grit surface finish after 40 h. In a previous study, a lack of substantial surface finish effect

was observed in TiAl alloys oxidized at 900 °C, comparing samples sanded to 600 grit with samples polished with diamond paste [25]. Other studies, however, were able to find a significant influence of the parameter on oxidation resistance, both negative [40–41] and positive [23, 42]. At shorter times, however, surface finish was relevant for the studied alloys. The main effects plots for 5 h are shown in Figure 8, which demonstrates that a rougher finishing (220) led to higher mass gain. This is likely related to the fact that the layer is initially planar, and grows in thickness only after covering the whole sample surface. In this stage, the surface condition is more relevant, because the metallic substrate is directly exposed to the atmosphere. When the oxide film becomes continuous, this effect is mitigated. The notion that rougher surfaces induce oxide nucleation agrees with previous findings [43] and explains why the rougher surface (higher surface area) increased mass gain. Furthermore, a previous study showed that rougher surfaces had a faster heating rate, and the difference in heating rate between a sample treated with 400 grit sandpaper and one treated with 600 grit sandpaper was significant [44]. Therefore, the higher heat absorption might increase mass gain. At 40 h (p-value = 0.03207), the associated influence is smaller than the one observed at 10 h (p-value = 0.00598), showing that surface finish is indeed more influential in early oxidation stages. Although the parameter did not affect the two alloys differently, its effect changed drastically with exposure time, which can help explain why the effect of initial roughness is so controversial in the literature.

Finally, the initial roughness parameter had a reduced effect on the metal/oxide roughness interface. Although all samples with an initial rougher surface (220 grit) ended up with a higher metal/oxide roughness, the difference was not statistically significant for Ra and only weakly significant for Rz. This result shows that

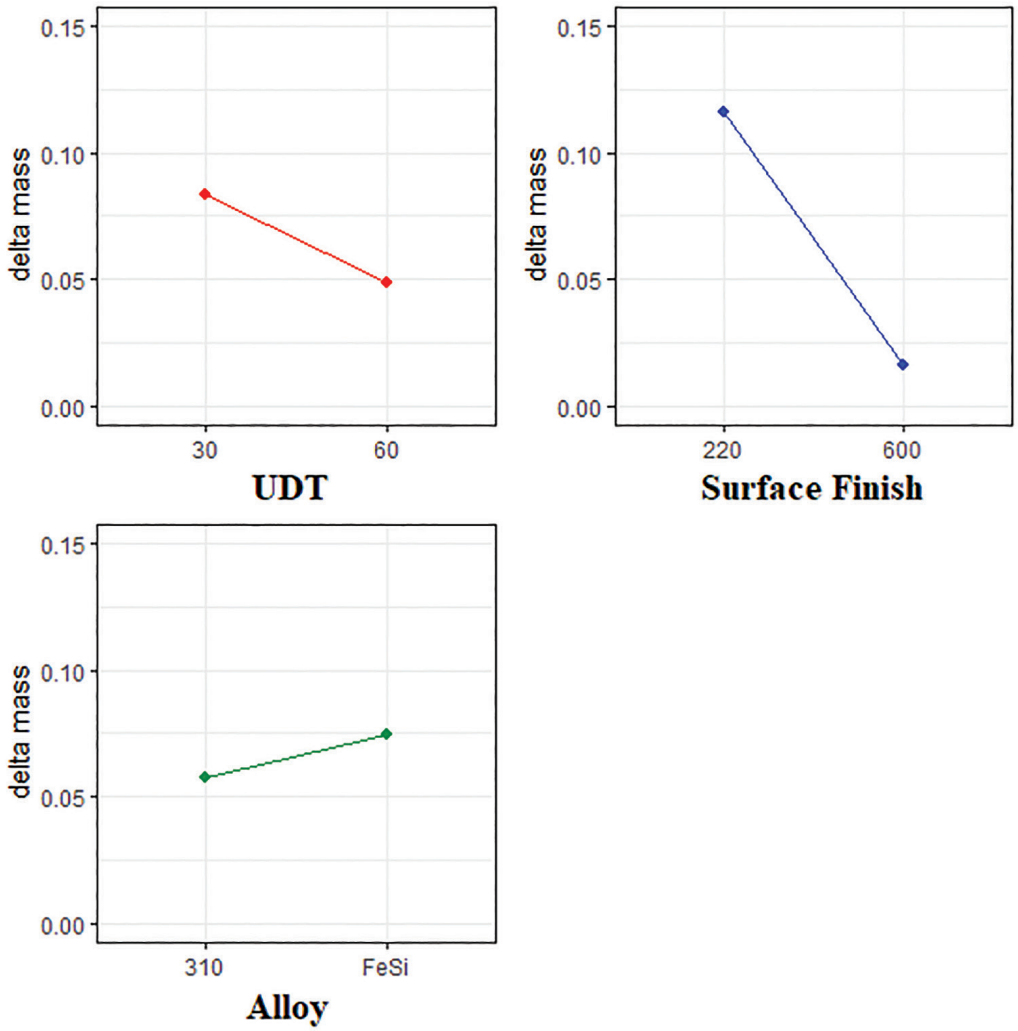

Figure 8: Main parameter effects and interaction plots for the mass variation response after 10 h of total dwell time. The extremities of each line indicate the average mass variation when the parameter is at a given level. Positive slopes indicate that changing the parameter from the lower to the upper level tends to increase mass variation, and negative slopes indicate that such a change tends to decrease mass variation, on average (note that the effect is not necessarily statistically relevant, as Table 5 shows).

the roughness increase during oxidation is only weakly affected by initial differences. Thus, this effect might explain the lack of relevance of the surface roughness parameter after 40 h of exposure. Before oxidation, samples sanded with 600 grit SiC paper had significantly lower Ra values, allowing the parameter to have a larger influence on oxidation behavior. As the roughness difference loses relevance during the oxidation process, the surface roughness effect on mass variation turns irrelevant. However, the indication that initial roughness has an effect, albeit weak, on final metal/oxide interface roughness depth (Rz) indicates that a larger difference in initial roughness could be effective in modifying oxidation behavior.

3.5. Upper dwell time influence

The UDT parameter was relevant in the last two observation points, with shorter 30-minute cycles leading to a higher mass variation. Analysis of Figure 2 shows that this represents a reduction in spallation. Since mass change is based on initial sample weight, when mass is lost by spallation a lower mass variation (Δm) value is calculated. Thus, a lower tendency to spall appears in statistical analyses as an increase in mass variation [31]. Although here the mass variation curves show that the UDT effect was related to spallation, it could also be evidence of a lower mass loss, in which case the results would be harder to interpret. Including gross mass variation as a response parameter could eliminate such doubts in future studies. Previously [30–31], no difference in mass gain was observed by changing UDT, but shorter UDTs led to an earlier onset of spallation, contrary to what was observed here. Longer dwell times were also shown to increase protective oxide growth time, with shorter cycles accelerating the onset of spallation (also the opposite of what was observed here). The authors considered shorter dwell times as 0.5, 1 and 2 h and longer dwell times as 4, 8 and 20 h [19]. For variations as low as the ones used in the present study (from 0.5 to 1h), the authors could not identify statistically relevant influences. In the present study, samples subjected to longer cycles showed signs of spallation close to the end of the experiment, after which statistical relevance was identified (85 and 100 h), while samples subjected to shorter cycles did not. This behavior can be attributed to interface defects caused by growth stresses, which lead to spallation during cooling [45]. For shorter cycles, lower stresses were developed as the oxide has less time to grow during each cycle. These stresses could be relieved during cooling without causing spallation. With longer cycles, the oxide develops larger stresses during the UDT, causing spallation during cooling. Previously, it was observed that shorter cycles caused less pronounced rumpling in surface layers during cyclic oxidation. This previous study ran longer tests with longer UDTs [46], but a similar effect could be responsible for the better result of samples subjected to shorter cycles observed here. The lack of interactions with the "Alloy" parameter shows that the tendency for UDT to increase spallation is independent of the spallation resistance of the two alloys. Thus, an increase in UDT reduces the spallation resistance of both alloys in equal measure. As for metal/oxide interface roughness, a higher number of cycles could increase thermal-shock-induced mechanical deformation in the substrate, an effect that was relevant in FeMnSiCrNi alloys [26]. In this study, a 30-minute UDT corresponded to twice as many thermal cycles as a 60-minute UDT. However, this did not cause a statistically relevant influence on interface roughness. Combined with the analysis of the alloy influence, this result shows that the roughness increase in the metal/oxide interface is related more to the chemical effect than the mechanical effect.

4. CONCLUSIONS

The effect of alloy composition, surface finish and UDT on the oxidation resistance of AISI 310 stainless steel and non-commercial Fe–5.9Si–3.85Cr–4.5Ni–0.79Mn–0.76C alloy at 950 °C were evaluated. The factorial design used shows potential as a substitute for designs commonly used in the cyclic oxidation field. In future studies, the design can be used to analyze these factors in different intervals, including new experimental parameters and other alloys. For the investigated alloys, a lack of interaction between experimental parameters was observed, but their main effects were relevant. The surface finish had a significant effect on early oxidation times, related to initial oxide growth. The effect decreased with time due, in part, to a metal/oxide interface roughness increase. UDT influence was relevant at the end of the test, showing that shorter cycle times increased the spallation resistance of both alloys. The metal/oxide interface roughness at the end of the test depended mostly on alloy composition, showing that a depletion-induced chemical effect is the main responsible for the increase in the interface roughness of both alloys and the initial surface roughness had a comparably small influence. Both the oxide layers of FeSiCr and AISI 310 contained chromium, chromium/manganese, and possibly silicon oxides. Mass variation results showed that the FeSiCr alloy was less prone to spallation despite initially gaining more mass than the conventional 310 alloy. The chemical-effect-induced roughness increase could have increased FeSiCr spallation resistance by improving metal/oxide adherence. Also, the lower CTE mismatch between oxide and substrate on the ferritic FeSiCr alloy decreased stresses generated during cooling, compared to the austenitic 310 alloy. This stress reduction, in turn, led to a lower spallation probability.

5. ACKNOWLEDGMENTS

The authors would like to thank CAPES (Coordination of Superior Level Staff Improvement) for providing a master's scholarship.

6. BIBLIOGRAPHY

[1] BALEIX, S., BERNHART, G., LOURS, P., "Oxidation and oxide spallation of heat resistant cast steels for superplastic forming dies", *Materials Science and Engineering: A*, v. 327, pp. 155–166, 2002. https://doi.org/10.1016/S0921-5093(01)01529-5

[2] SABIONI, A.C.S., HUNTZ, A.-M., LUZ, E.C., *et al.*, "Comparative study of high temperature oxidation behaviour in AISI 304 and AISI 439 stainless steels", *Materials Research*, v. 6, pp. 179–185, 2003. https://doi.org/10.1590/S1516-14392003000200012

[3] SMIALEK, J.L., BONACUSE, P.J., "Compositional effects on the cyclic oxidation resistance of conventional superalloys", *Materials at High Temperatures*, v. 33, pp. 489–500, 2016. https://doi.org/10.1080/09603409.2016.1160501

[4] SOUZA, V.F., ARAÚJO, A.J., SANTOS, J.L.N., *et al.,* "Kinetics Oxidation and Characterization of Cyclically Oxidized Layers at High Temperatures for FeMnSiCrNiCe and FeSiCrNi Alloys", *Materials Research*, v. 20, pp. 365–373, 2017. https://doi.org/10.1590/1980-5373-mr-2017-0098

[5] HUNTZ, A.M, BAGUE, V., BEAUPLÉ, G., *et al.,* "Effect of silicon on the oxidation resistance of 9% Cr steels", *Applied Surface Science*, v. 207, pp. 255–275, 2003. https://doi.org/10.1016/S0169-4332(02)01505-2

[6] EKLUND, J, JÖNSSON, B., PERSDOTTER, A., *et al.,* "The influence of silicon on the corrosion properties of FeCrAl model alloys in oxidizing environments at 600 °C", *Corrosion Science*, v. 144, pp. 266–276, 2018. https://doi.org/10.1016/j.corsci.2018.09.004

[7] PEREZ, T., MATHIEU, S., PARSA, Y., *et al.*, "About the Synergetic Influence of Manganese and Silicon on the Oxidation Rate of Chromia Forming Nickel-Based Model Alloys at 1050 °C", *Oxidation of Metals*, v. 94, pp. 235–249, 2020. https://doi.org/10.1007/s11085-020-09988-1.

[8] GORR, B., MUELLER, F., CHRIST, H.-J., *et al.*, "High temperature oxidation behavior of an equimolar refractory metal-based alloy 20Nb 20Mo 20Cr 20Ti 20Al with and without Si addition", *Journal of Alloys and Compounds*, v. 688, pp. 468–477, 2016. https://doi.org/10.1016/j.jallcom.2016.07.219

[9] SHAJAHAN, S., KUMAR, A., CHOPKAR, M., *et al.*, "Oxidation study of CoCrCuFeNiSix high entropy alloys", *Materials Research Express*, v. 7, pp. (2020) 016532, 2020. https://doi.org/10.1088/2053-1591/ab640a

[10] KAI, W., CHENG, F.P., LIAO, C.Y., *et al.*, "The oxidation behavior of the quinary FeCoNiCrSix high-entropy alloys", *Materials Chemistry and Physics*, v. 210, pp. 362–369, 2018. https://doi.org/10.1016/j.matchemphys.2017.06.017

[11] CASTRO, D.B.V., ROSSINO, L.S., MALAFAIA, A.M.S., *et al.*, "Influence of annealing heat treatment and Cr, Mg, and Ti alloying on the mechanical properties of high-silicon cast iron", *Journal of Materials Engineering and Performance*, v. 20, pp. 1346–1354, 2011. https://doi.org/10.1007/s11665-010-9733-y

[12] KIM, B.H., SHIN, J.S., LEE, S.M., *et al.,* "Improvement of tensile strength and corrosion resistance of high-silicon cast irons by optimizing casting process parameters", *Journal of Materials Science*, v. 42, pp. 109–117, 2007. https://doi.org/10.1007/s10853-006-1081-9

[13] MALAFAIA, A.M.S., MILAN, M.T., OMAR, M., *et al.*, "Oxidation and abrasive wear of Fe–Si and Fe–Al intermetallic alloys", *Journal of Materials ScienceI*, v. 45, pp. 5393–5397, 2010. https://doi.org/10.1007/s10853-010-4591-4

[14] BAMBA, G., WOUTERS, Y., GALERIE, A., *et al.*, "Thermal oxidation kinetics and oxide scale adhesion of Fe-15Cr alloys as a function of their silicon content", *Acta Materialia*, v. 54, pp. 3917–3922, 2006. https://doi.org/10.1016/j.actamat.2006.04.023

[15] PEREIRA, J.N., SOUZA, V.F., MALAFAIA, A.M.S "Evaluation of Si Content in FeSiCrNi Alloys Containing Carbon on Cyclic Oxidation Resistance at 950 °C", *Oxidation of Metals,* v. 96, pp 453–468, 2021. https://doi.org/10.1007/s11085-021-10035-w

[16] NICHOLLS, J.R., BENNETT, M.J., "Cyclic oxidation – guidelines for test standardisation, aimed at the assessment of service behaviour", *Materials at High Temperatures*, v. 17, pp. 413–428, 2000. https://doi.org/10.1179/mht.2000.17.3.005

[17] HAANAPPEL, V.A.C., STROOSNIJDER, M.F., "The Importance of Relevant Experimental Parameters for High Temperature Cyclic Oxidation Experiments An attempt for a checklist", In: Schütze, M., Quadakkers, W.J. (org), *Cyclic Oxidation of High Temperature Materials.* Boca Raton: CRC Press, 1999. pp. 225–239

[18] PHALNIKAR, C.A., EVANS, E.B., BALDWIN, W.M., "High Temperature Scaling of Cobalt-Chromium Alloys", *Journal of The Electrochemical Society*, v. 103, pp. 429–438, 1956. https://doi.org/10.1149/1.2430374

[19] NIEWOLAK, L., MALESSA, M., COLEMAN, S.Y., *et al.,* "Influence of cycling parameter variation on thermal cyclic oxidation testing of high temperature materials (COTEST)", *Materials and Corrosion*, v. 57, pp. 31–42, 2006. https://doi.org/10.1002/maco.200503892

[20] SCHÜTZE, M., MALESSA, M., *Standardization of thermal cyclic exposure testing*. Cambridge: Woodhead Publishing, 2007.

[21] ZUREK, J., QUADAKKERS, W.J., "Effect of Surface Condition on Steam Oxidation of Martensitic Steels and Nickel-Based Alloys", *Corrosion*, v. 71, pp. 1342–1359, 2015. https://doi.org/10.5006/1859

[22] OSGERBY, S., "Survey of existing test procedures and experimental facilities", In: Schütze, M., Malessa, M. (org), *Standardisation of Thermal Cycling Exposure Testing*. Cambridge: Woodhead Publishing, 2007. pp. 3–10.

[23] GUTTMANN, V., HUKELMANN, F., GRIFFIN, D., *et al*., "Studies of the influence of surface pre-treatment on the integrity of alumina scales on MA 956", *Surface and Coatings Technology*, v. 166, pp. 72–83, 2003. https://doi.org/10.1016/S0257-8972(02)00777-6

[24] DUDZIAK, T., ŁUKASZEWICZ, M., SIMMS, N., *et al.*, "Steam oxidation of TP347HFG , super 304H and HR3C – analysis of significance of steam flowrate and specimen surface finish", *Corrosion Engineering, Science and Technology*, v. 50, pp. 272–282, 2014. https://doi.org/10.1179/1743278214Y.0000000222

[25] DETTENWANGER, F., SCHUMANN, E., RUHLE, M., *et al.*, "Microstructural study of oxidized γ-TiAl", *Oxidation of Metals*, v. 50, pp. 269–307, 1998. https://doi.org/10.1023/A:1018892422121

[26] RABELO, L.F.P., SILVA, R., DELLA ROVERE, C.A., *et al.*, "Metal/oxide interface roughness evolution mechanism of an FeMnSiCrNiCe shape memory stainless steel under high temperature oxidation", *Corrosion Science*, v. 163, 108228, 2020. https://doi.org/10.1016/j.corsci.2019.108228.

[27] MALAFAIA, A.M.S., OLIVEIRA, M.F., "Anomalous cyclic oxidation behaviour of a Fe–Mn–Si–Cr–Ni shape memory alloy", *Corrosion Science*, v. 119, pp. 112–117, 2017. https://doi.org/10.1016/j.corsci.2017.02.026

[28] MALAFAIA, A.M.S., NASCIMENTO, V.R., SOUZA, L.M., *et al.*, "Anomalous cyclic oxidation behaviour of an Fe-Mn-Si-Cr-Ni alloy - A finite element analysis", *Corrosion Science*, v. 147, pp. 223–230, 2019.

[29] WRIGHT, I.G., PINT, B.A., TORTORELLI, P.F., "High-Temperature Oxidation Behavior of ODS – Fe_3 Al", *Oxidation of Metals*, v. 55, pp. 333–357, 2001. https://doi.org/10.1023/A:1010316428752

[30] COLEMAN, S., MCGEENEY, D., PETTERSSON, R., "Statistical analysis of cyclic oxidation data", In: Schütze, M., Malessa, M., *Standardisation of Thermal Cycling Exposure Testing*. Cambridge: Woodhead Publishing, 2007. pp. 17–37.

[31] NIEWOLAK, L., QUADAKKERS, W.J., "Investigation of the influence of parameter variation in long dwell thermal cycling oxidation", In: Schütze, M., Malessa, M., *Standardisation of Thermal Cycling Exposure Testing*. Cambridge: Woodhead Publishing, 2007. pp. 110–123.

[32] PINT, B.A., TORTORELLI, P.F., WRIGHT, I.G., "Effect of cycle frequency on high-temperature oxidation behavior of alumina-forming alloys", *Oxidation of Metals*, v. 58, pp. 73–101, 2002. https://doi.org/10.1023/A:1016064524521

[33] POQUILLON, D., MONCEAU, D., "Application of a Simple Statistical Spalling Model for the Analysis of High-Temperature, Cyclic-Oxidation Kinetics Data", *Oxidation of Metals*, v. 59, pp. 409–431, 2003. https://doi.org/10.1023/A:1023004430423

[34] MOCCARI, A., ALI, S.I., "Studies on the Oxidation and Spalling Resistance of Austenitic Stainless Steels", *British Corrosion Journal*, v. 14, pp. 91–96, 1979. https://doi.org/10.1179/000705979798275870

[35] TSAI, W.-T., HUANG, K.-E., "Microstructural aspect and oxidation resistance of an aluminide coating on 310 stainless steel", *Thin Solid Films*, v. 366, pp. 164–168, 2000. https://doi.org/10.1016/S0040-6090(00)00723-9

[36] STOTT, F.H., WEI, F.I., "High temperature oxidation of commercial austenitic stainless steels*", Materials Science and Technology*, v. 5, pp. 1140–1147, 1989. https://doi.org/10.1179/mst.1989.5.11.1140

[37] YUREK, G.J., EISEN, D., GARRATT-READ, A., "Oxidation behavior of a fine-grained rapidly solidified 18-8 stainless steel", *Metallurgical Transactions A*, v. 13, pp. 473–485, 1982. https://doi.org/10.1007/BF02643355

[38] YANG, C.-H., LIN, S.-N., CHEN, C.-H., *et al.*, "Effects of Temperature and Straining on the Oxidation Behavior of Electrical Steels", *Oxidation of Metals*, v. 72, pp. 145–157, 2009. https://doi.org/10.1007/s11085-009-9152-3

[39] CHUN, C.M., RAMANARAYANAN, T.A., "Corrosion Resistance of a High-Silicon Alloy in Metal-Dusting Environments", *Oxidation of Metals*, v. 67, pp. 215–234, 2007. https://doi.org/10.1007/s11085-007-9052-3

[40] OSTWALD, C., GRABKE, H.J., "Initial oxidation and chromium diffusion. I . Effects of surface working on 9 – 20 % Cr steels", *Corrosion Science*, v. 46, pp. 1113–1127, 2004. https://doi.org/10.1016/j.corsci.2003.09.004

[41] SUDBRACK, C.K., BECKETT, D.L., MACKAY, R.A., "Effect of Surface Preparation on the 815 ° C Oxidation of Single- Crystal Nickel-Based Superalloys", *The Journal of The Minerals, Metals & Materials Society*, v. 67, pp. 2589–2598, 2015. https://doi.org/10.1007/s11837-015-1639-6

[42] PLATT, P., ALLEN, V., FENWICK, M., *et al.*, "Observation of the effect of surface roughness on the oxidation of Zircaloy-4", *Corrosion Science*, v. 98, pp. 1–5, 2015. https://doi.org/10.1016/j.corsci.2015.05.013

[43] TAYLOR, P., MCEACHERN, R.J., DOERN, D.C., *et al.*, "The influence of specimen roughness on the rate of formation of U3O8 on UO2 in air at 250°C", *Journal of Nuclear Materials*, v. 256, pp. 213–217, 1998. https://doi.org/10.1016/S0022-3115(98)00063-4

[44] AUINGER, M., EBBINGHAUS, P., BLÜMICH, A., *et al.*, "Effect of surface roughness on optical heating of metals", *Journal of the European Optical Society: Rapid Publications*, v. 9, 14004, 2014. https://doi.org/10.2971/jeos.2014.14004

[45] HE, M., EVANS, A., HUTCHINSON, J., "Effects of morphology on the decohesion of compressed thin films", *Materials Science and Engineering: A*, v. 245, pp. 168–181, 1998. https://doi.org/10.1016/S0921-5093(97)00848-4

[46] TOLPYGO, V.K., CLARKE, D.R., "Surface rumpling of a (Ni , Pt) Al bond coat induced by cyclic oxidation", *Acta Materialia*, v. 48, pp. 3283–3293, 2000.